Inorganic Chemistry

ARTICLE

pubs.acs.org/IC

# Synthesis and $Cu^{II}$ Coordination Chemistry of a Patellamide Derivative: Consequences of the Change from the Natural Thiazole/Oxazoline to the Artificial Imidazole Heterocycles

Peter Comba,*[,†] Nina Dovalil,[†] Graeme R. Hanson,[‡] and Gerald Linti[†]

[†]Universität Heidelberg, Anorganisch-Chemisches Institut, D-69120 Heidelberg, Germany

[‡]Centre for Advanced Imaging, The University of Queensland, Brisbane, Queensland 4072, Australia

Supporting Information

**ABSTRACT:** The synthesis and $Cu^{II}$ coordination chemistry of the cyclic pseudo-octapeptide $H_4pat^1$, a dimethyl-imidazole analogue of naturally occurring cyclic peptides (patellamide A−F, ascidiacyclamide) is reported. Substitution of the oxazoline and thiazole heterocycles by dimethyl-imidazoles leads to a slightly different structure of the macrocycle in the solid state. The $Cu^{II}$ coordination chemistry of $H_4pat^1$, monitored with high-resolution electrospray mass spectrometry, spectrophotometric titrations, and EPR spectroscopy, revealed the presence of both mono- and dinuclear $Cu^{II}$ complexes. The dimethyl-imidazole analogue shows a high cooperativity in $Cu^{II}$ coordination, that is, the preferred formation of dinuclear complexes. The dinuclear unbridged $Cu^{II}$ complexes of $H_4pat^1$ have unusual EPR features, reminiscent of those of patellamide D: the dipole−dipole interaction of the $Cu^{II}$ centers is negligible due to the "magic angle" orientation of the two $Cu^{II}$ ions. Density functional theory calculations (DFT) are used to model the structures of the $Cu^{II}$ complexes, and the structural assignments from the spectroscopic investigations are supported by the optimized and by X-ray structures of the metal-free macrocycle and dinuclear $Cu^{II}$ complexes of $H_4pat^1$. The rigidity of the dimethyl-imidazole rings has a significant effect on the structures of the metal-free ligands and $Cu^{II}$ complexes and therefore changes the properties of these compounds. This may explain why Nature has chosen the thiazole−oxazoline combination for the patellamides and ascidiacyclamide.

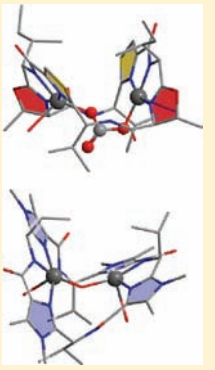

## 1. INTRODUCTION

Cyclic peptides of variable size and shape and with differing donor sets (primarily peptide, thiazole, and oxazoline nitrogen atoms) are abundant in the ascidians of the Pacific and Indian oceans. Particularly well studied are the [24]azacrown-8 (pseudo-octapeptide) macrocycles patellamide A−F and ascidiacyclamide ($H_4asc$) of *Lissoclinum patella* (Scheme 1).[1−4] The natural macrocycles are built up from oxazoline and thiazole rings that are alternatingly connected by D- and L-amino acids ($R^*$ or $S^*$ configuration at $C_\alpha$). The five-membered heterocyclic rings result from condensation of serine, threonine, and cysteine side chains with the preceding carbonyl groups in the peptide sequence; natural cyclic peptides with imidazole groups have not yet been isolated. This may be because the diaminopropanoic acid, which formally is the amine-analogue of serine, is rare in natural systems.[5,6] Solid-state and solution structures and dynamics of metal-free natural and synthetic cyclic pseudo-octapeptides,[7−12] the biosynthesis[13] and pharmaceutical activities[14] of the natural peptides, and the $Cu^{II}$ complexes of natural and synthetic compounds have been reported.[2,15−22]

The size, geometric arrangement, and set of nitrogen donor atoms in the ring of the cyclic peptides makes them well suited for the coordination to metal ions.[17,18,23−28] NMR studies have shown that the conformation of the metal-free macrocycles in solution is identical to that in the solid state.[29−34] The macrocycles are able to bind divalent metal ions such as $Zn^{II}$ and $Cu^{II}$, with a distinct preference for $Cu^{II}$, which leads to the assumption that $Cu^{II}$ is the biologically relevant metal ion.[35] $Cu^{II}$ is coordinated to two heterocyclic and one amide nitrogen donor of a deprotonated amide group, forming a $N_{het}-N_{amide}-N_{het}$ binding motif. The formation of the mono- and dinuclear $Cu^{II}$ complexes involves two metal-ion-assisted deprotonation steps of the amide nitrogen donors, leading to a drop in pH and the necessity to add base to achieve complete complexation.

Depending on the connecting amino acids, the cyclic pseudo-octapeptides adopt different conformations.[32,36] Symmetrical peptides, such as $H_4asc$, take on a saddle-shaped conformation (type I, Figure 1) with the thiazole and oxazoline rings located alternately at each corner of the rectangular ring and the eight nitrogens pointing toward the inside of the molecule in a well-preorganized arrangement for the coordination to two metal ions. Asymmetric peptides on the other hand, for example, patellamide D ($H_4patD$, see Scheme 1), adopt a "figure of eight" conformation (Figure 1, type IV), stabilized by two trans-annular $N-H\cdots O{=}C$ (amide) and two trans-annular $N-H\cdots O_{oxa}$ (oxazoline ring) hydrogen bonds.[37] In this conformation, the oxazoline nitrogen atoms point toward the outside of the macrocycle.

**Received:** March 8, 2011
**Published:** May 12, 2011

**Scheme 1. Chemical Structures and Stereochemical Configurations of Cyclic Peptides**

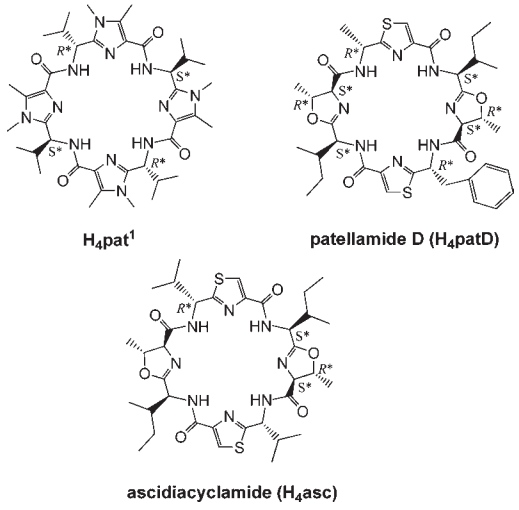


The macrocycle $H_4pat^1$ is a simplified model for the symmetrical patellamides, with four dimethyl-imidazole heterocycles, alternatingly connected by D- and L-valines. Valine was used as a bridging amino acid to minimize steric effects of the side chains on the $Cu^{II}$ coordination chemistry. The heterocycles provide two of the three nitrogen donors and therefore strongly influence the coordination chemistry of the macrocycles, in particular also the complex stabilities.[38] Compared with the natural systems, $H_4pat^1$ is more rigid (oxazoline vs. dimethyl-imidazole), and there are considerable differences in the nucleophilicity of the various donor groups ($pK_a$(oxazole) = 0.8, $pK_a$(thiazole) = 2.5, $pK_a$(oxazoline) = 4.8, $pK_a$(N-methylimidazole) = 7).[16] Structures and solution properties of the $Cu^{II}$ complexes of $H_4pat^1$ are discussed on the basis of spectroscopic data (ESI-MS, UV−vis, EPR, CD), spectra simulations, spectrophotometric titrations, and DFT- and MM-based model calculations, and are compared with the $Cu^{II}$ coordination chemistry of the natural pseudo-octapeptides $H_4$asc and $H_4$patD. As a consequence of the low solubility of $H_4pat^1$ in water, all experiments were performed in methanol.

## 2. RESULTS AND DISCUSSION

**2.1. Cyclic Pseudo-peptide Synthesis.** $H_4pat^1$ was prepared in analogy to published procedures in a seven-step synthesis with an overall yield of 15% (Scheme 2).[39]

**2.2. Copper(II) Coordination Chemistry.** *2.2.1. Mass Spectrometry.* High-resolution electrospray-ionization mass spectrometry (ESI-MS) was used to identify charged complexes in methanolic solutions of $H_4pat^1$, $Cu^{II}(Otf)_2$ (Otf = trifluoromethanesulfonate), and base $[(n\text{-}Bu_4N)(OMe)]$ (details of the experimental and calculated exact masses are given as Supporting Information). The relevant $Cu^{II}$ species were monopositive complex cations throughout, and no negatively charged complexes were detected. Spectra featuring signals for the protonated metal-free macrocycle at $m/z$ 773.4936 $[H_5pat^1]^+$, together with those of the mononuclear complexes at $m/z$ 834.4081 $[Cu^{II}(H_3pat^1)(H_2O)]^+$, 852.4189 $[Cu^{II}(H_3pat^1)(H_2O)]^+$ and the dinuclear complex at $m/z$ 913.3318 $[Cu^{II}_2(H_2pat^1(OH)^+$, were obtained from solutions with varying macrocycle/$Cu^{II}$/base ratios.[40] The signal intensity of

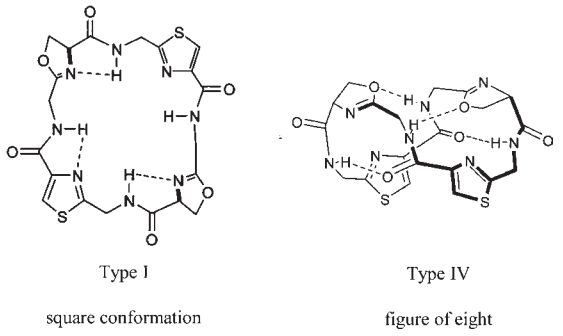


**Figure 1.** Conformations (square and figure of eight) of ascidiacyclamide and the patellamides adopted in solution and in the solid state.[32,35,36]

**Scheme 2. Synthesis of $H_4pat^1$**[a]

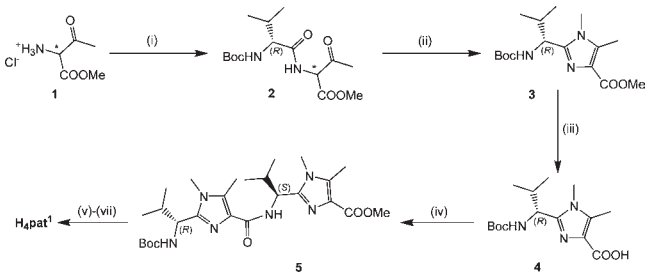


[a] Reagents and conditions: (i) Boc-(*R*)-Val-OH, $ClCOO^iBu$, *N*-methylmorpholin, tetrahydrofuran (THF), r.t., 87%; (ii) $MeNH_2$, AcOH, xylene, reflux, 51%; (iii) NaOH, MeOH/dioxane, r.t., quantitative; (iv) TFA-(*S*)-Val-imidazole-methoxide, pentafluorophenyl diphenyl phosphinate (FDPP), ethylendiisopropyl amine (EDIPA), acetonitrile (ACN), r.t., 68%; (v) NaOH, MeOH/dioxane, r.t., quantitative; (vi) trifluoracetic acid (TFA), dichloromethane (DCM), 0 °C → r.t., quantitative; (vii) FDPP, EDIPA, ACN, r.t., 51%.

the dinuclear complex increases with the base concentration. Interestingly, signals assigned to the dinuclear hydroxo-complex of $H_4pat^1$ $[Cu^{II}_2(H_2pat^1)(OH)]^+$ could even be observed in the absence of base at a macrocycle:$Cu^{II}$ ratio of 1:1, indicating a strong cooperativity, that is, preorganization for the coordination of a second $Cu^{II}$ ion by binding of the first. At low $Cu^{II}$ concentrations, a nearly complete formation of the dinuclear complex occurs. Increased $Cu^{II}$ concentrations acidify the solution by deprotonation of the amide binding sites, and this leads to a preference for the mononuclear complex $[Cu^{II}(H_3pat^1)]^+$ and solvated $Cu^{II}$. This complexation behavior is qualitatively identical to that reported for $H_4$asc and $H_4$patD.[24,26]

*2.2.2. Spectrophotometric Titrations.* In contrast to the $Cu^{II}$ complexes of the natural systems, those of $H_4pat^1$ are racemic mixtures of enantiomers, and therefore, solutions of the mono- and dinuclear $Cu^{II}$ complexes of $H_4pat^1$ are CD silent.

UV−vis titrations of $Cu^{II}$ to solutions of $H_4pat^1$ and of base $[(n\text{-}Bu_4N)(OMe)]$ to solutions of $H_4pat^1$:$Cu^{II}$ = 1:2 are shown in Figure 2. Upon addition of $Cu^{II}$, a band at 714 nm appears; this is a combination of the bands from the mono- and dinuclear $Cu^{II}$ complexes of $H_4pat^1$ and solvated $Cu^{II}$ ($[Cu^{II}(MeOH)_n]^{2+}$; $\lambda_{max}$ = 840 nm, see Supporting Information for a Gaussian analysis), and it linearly increases with the $Cu^{II}$ concentration until 2 equiv (Figure 2a, inset). Addition of base shifts the complexation equilibrium to the dinuclear complex, observable


dx.doi.org/10.1021/ic2004694 |*Inorg. Chem.* 2011, 50, 5165–5174

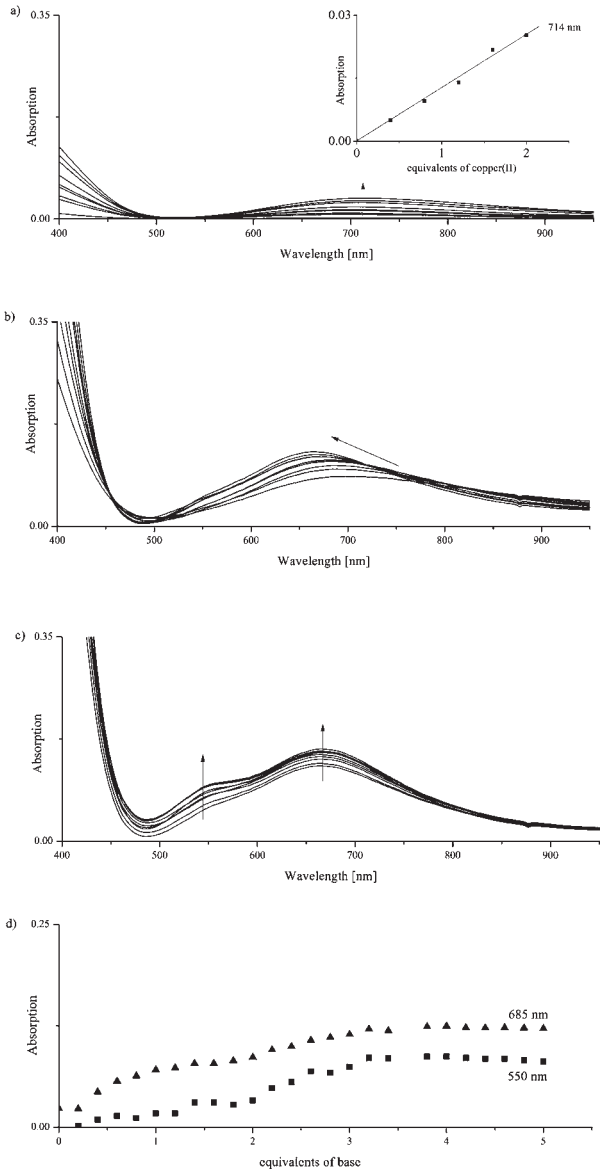


**Figure 2.** UV−vis spectra in methanol ($c(H_4pat^1)$ = 1.25 mM; base ($n$-$Bu_4N$)(OMe)). Titration of (a) 0−2 equiv of $Cu^{II}$ (0.2 equiv steps) to a solution of $H_4pat^1$ with insert showing absorbance at 714 nm versus equivalents of $Cu^{II}$, (b) 0−2 equiv of base (0.2 equiv steps) to an $H_4pat^1$:$Cu^{II}$ 1:2 solution, and (c) 2−5 equiv of base (0.2 equiv steps) to an $H_4pat^1$:$Cu^{II}$ 1:2 solution; (d) absorbance of the bands at $\lambda$ = 685 and 550 nm as a function of base.

at $\lambda_{max}$ = 685 nm (Figure 2b). At base concentrations ≥ 2 equiv, a shoulder at 550 nm evolves (Figure 2c, $\varepsilon$ = 81 $M^{-1}$ $cm^{-1}$), and this must be due to the formation of a new species (structural rearrangement of the complex, see section on EPR below).[41] From the combination of the UV−vis and ESI-MS spectra, we conclude that initially, the dinuclear $Cu^{II}$ complex $[Cu^{II}_2(H_2pat^1)]^{2+}$ ($\lambda_{max}$ = 685 nm) is formed and is subsequently converted to a hydroxo complex, that is, to $[Cu^{II}_2(H_2pat^1)(OH)]^{+}$.

*2.2.3. EPR Spectroscopy.* X-band EPR spectra of solutions in methanol, with different ratios of $Cu^{II}$, $H_4pat^1$, and base, were recorded to validate this interpretation and to provide more detailed structural insights. When $H_4pat^1$ and base are added to a solution of $Cu^{II}$ in methanol (Figure 3a), a new set of resonances

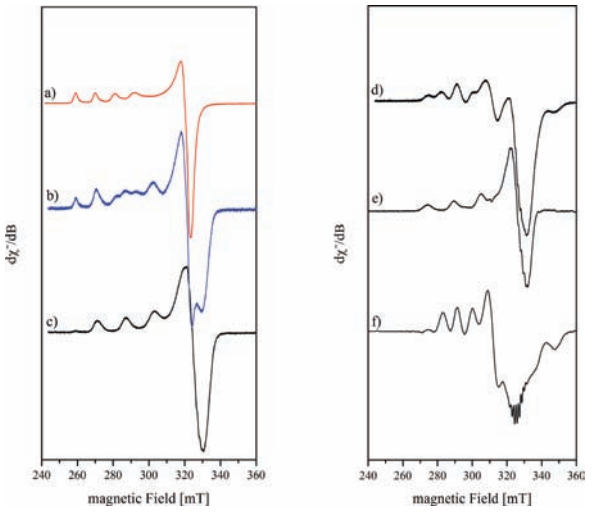


**Figure 3.** Experimental X-band EPR spectra (methanol, $c(H_4pat^1)$ = 1.25 mM): (a) solvated $Cu^{II}$ $[Cu^{II}(MeOH)_n]^{2+}$, $T$ = 145 K, $\nu$ = 9.427799 GHz; (b) $H_4pat^1$:$Cu^{II}$:$MeO^-$ 1:2:1, $T$ = 10 K, $\nu$ = 9.377228 GHz; (c) $H_4pat^1$:$Cu^{II}$:$MeO^-$ 1:2:2, $T$ = 4.5 K, $\nu$ = 9.375067 GHz; (d) $H_4pat^1$:$Cu^{II}$:$MeO^-$ 1:2:3, $T$ = 50 K, $\nu$ = 9.377548 GHz: (e) pure "apparent monomer" species present in spectrum d derived from spectral subtraction of the spectrum with 3 equiv of base from the spectrum with 4 equiv of base (see Supporting Information for the 1:2:4 spectrum); (f) dinuclear species present in spectrum d, derived from spectral subtraction. The resonances at ∼320 mT arise from a monomeric impurity that could not be completely eliminated through spectral subtraction.

between 260 and 340 mT appears (Figure 3b, $H_4pat^1$:$Cu^{II}$:base 1:2:1). Upon addition of a second equivalent of base, the resonances of solvated (uncomplexed) $Cu^{II}$ almost completely disappear, and the spectrum consists of the new set of resonances (Figure 3c).

This spectrum (Figure 3c) is characteristic of a single magnetically isolated $Cu^{II}$ center, which has a significantly different set of spin Hamiltonian parameters compared with those of solvated $Cu^{II}$ (see Table 1; e.g., $g_{||}$ = 2.26 (coordinated $Cu^{II}$) vs 2.43 (solvated $Cu^{II}$), the corresponding $^{63}Cu$ hyperfine values are $A_{||}$ = 166.88 vs 108.00 × $10^{-4}$ $cm^{-1}$), indicating that the 2 equiv of $Cu^{II}$ are fully coordinated to $H_4pat^1$. The resonances of the spectrum in Figure 3c are due to a single species and therefore must arise from a dinuclear $Cu^{II}$ complex of $H_4pat^1$. In agreement with the ESI-MS and UV−vis spectra, this is $[Cu^{II}_2(H_2pat^1)(OH)]^{2+}$

In general, the EPR spectrum of a randomly oriented mononuclear $Cu^{II}$ complex consists of a set of four resonances each in the $x$, $y$, and $z$ directions (parallel and perpendicular to $z$ in axial systems; $I$ = $^3/_2$, $S$ = $^1/_2$), while the spectra of dipole−dipole coupled dinuclear complexes ($J_{iso}$ ≈ 0, eq 2) have a set of seven resonances (coupling of each electron to both nuclei) along these principal directions. An "apparent mononuclear spectrum" such as that in Figure 3c is observed when the dipole−dipole interaction between the metal centers is negligible. This occurs, when either the internuclear $Cu^{II}\cdots Cu^{II}$ distance is large (>10 Å) or when the $g$ and $A$ matrices of the two $Cu^{II}$ ions are oriented at the *magic angles*, that is, Euler angles of α = 54.7° and $\beta$ = 37.5°.[25] Anisotropic exchange coupling can also contribute to the interaction of the $Cu^{II}$ centers and can help to suppress the dipole−dipole coupling.


dx.doi.org/10.1021/ic2004694 |*Inorg. Chem.* 2011, 50, 5165–5174

**Table 1. Anisotropic Spin Hamiltonian Parameters of Solvated $Cu^{II}$ ($[Cu^{II}(MeOH)_n]^{2+}$)[46] and of the bridged and unbridged dinuclear $Cu^{II}$ complexes in comparison with dinuclear complexes of $H_4$asc and $H_4$pat[1]**

| | $Cu^{II}$ (solv) | $[Cu^{II}_2(H_2pat^1)(H_2O)]^{2+}$ | $[Cu^{II}_2(H_2pat^1)(OH)]^{+}$ | $[Cu^{II}_2(H_2pat^1)(\mu\text{-}OH)]^{+}$ | $[Cu^{II}_2(H_2asc)(\mu\text{-}CO_3)]$[26] | $[Cu^{II}_2(H_2patD)(H_2O)]^{2+}$[25] |
|---|---|---|---|---|---|---|
| $g_x$ | 2.084 | 2.0719 | 2.0503 | 2.027 | 2.10 | 2.06 |
| $g_y$ | 2.084 | 2.0456 | 2.0539 | 2.033 | 2.10 | 2.06 |
| $g_z$ | 2.428 | 2.258 | 2.2600 | 2.260 | 2.310 | 2.242 |
| $A_x(^{63}Cu)$[a] | 15.000 | 4.019 | 12.6896 | 25 | 70 | 11.0 |
| $A_y(^{63}Cu)$[a] | 15.000 | 4.423 | 9.2275 | 24 | 70 | 11.0 |
| $A_z(^{63}Cu)$[a] | 108.00 | 166.88 | 161.64 | 189 | 111 | 160 |
| $A_{x/y/z}(^{14}N_{het})$[a,b] | | 8.00/11.00/10.00 | 6.00/9.00/10.00 | | | |
| $A_{x/y/z}(^{14}N_{amide})$[a,b] | | 15.00/13.00/13.00 | 13.00/12.00/12.00 | | | |
| Cu···Cu [Å] | | 4.0[c] | 4.0[c] | 3.8 | 3.6 | 6.8 |
| $\alpha/\beta/\gamma$ (Cu1) | | −5/−25/−30 | −5/−25/−30[d] | −55/−23/0 | 144/5/5 | 54.7/45/0 |
| $\alpha/\beta/\gamma$ (Cu2) | | 5/25/30 | 5/25/30 | 55/+23/0 | 0/0/0 | |
| $J_{iso}$ [$cm^{-1}$][d] | | $1 \times 10^{-3}$ | $9 \times 10^{-4}$ | 2.6 | 3.2 | |
| $D_{exc}$ [$cm^{-1}$][e] | | 0.0935 | 0.09378 | 0.112 | | |
| $(E/D)_{exc}$ [$cm^{-1}$][e] | | 0.02 | 0.02 | 0.20 | | |

[a] [$10^{-4}$ $cm^{-1}$]. [b] Simulated spectra of $H_4$pat[1] included two magnetically identical heterocyclic nitrogen nuclei. [c] Determined from the simulation of the spectra with Molecular Sophe. [d] Equation 2. [e] Diagonal elements of the anisotropic **J** matrix are $J_x = -D_{exc}/3 - E_{exc}$; $J_y = -D_{exc}/3 + E$; $J_z = 2D_{exc}/3$.

**Scheme 3. $Cu^{II}$ Complexation Equilibria of $H_4$pat[1] (S = Solvent = Methanol)[40]**

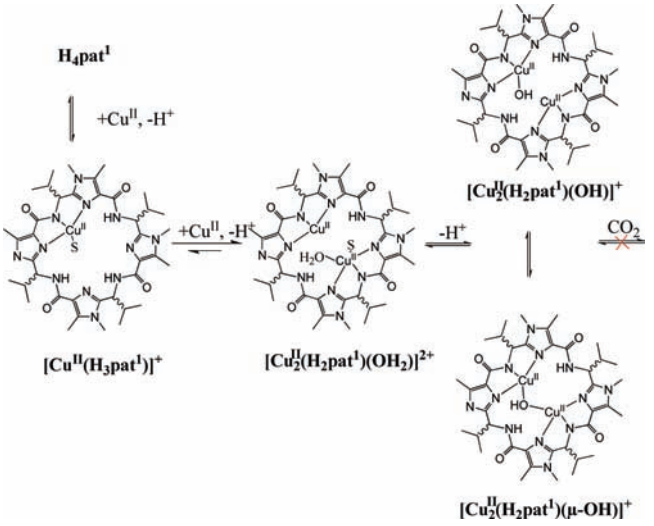


As expected from the UV−vis spectra (see Figure 2c), upon addition of a third equivalent of base, there also is a significant change in the EPR spectra. The spectrum in Figure 3d is, in agreement with the electronic spectra, due to a mixture of two different dinuclear species. While one of the species (Figure 3e) has an "apparent mononuclear EPR spectrum" and therefore has a structure similar to that of the dinuclear complex with the spectrum in Figure 3c, the other species has a different structure with a typical dipole−dipole coupled spectrum (spectra obtained by spectral subtraction of spectra recorded at different base concentrations).[42] There was no evidence from ESI-MS, spectrophotometric titrations, and EPR spectroscopy for the formation of a carbonato-bridged dinuclear $Cu^{II}$ complex, which has previously been observed in the $Cu^{II}$ coordination chemistry of $H_4$patD and $H_4$asc. The combination of all these results can be interpreted with the complexation equilibria in Scheme 3.

At low base concentrations, a dinuclear $Cu^{II}$ aqua complex is formed $[Cu^{II}_2(H_2pat^1)(OH_2)]^{2+}$. The orientation of the two $Cu^{II}$ centers along the magic angles leads to an "apparent mononuclear EPR spectrum". Addition of more than 3 equiv of base leads to the formation of two structurally different hydroxo complexes, one with a terminal hydroxide, $[Cu^{II}_2(H_2pat^1)(OH)]^{+}$, and the other with a hydroxo bridge, $[Cu^{II}_2(H_2pat^1)(\mu\text{-}OH)]^{+}$. In the former complex, the two $Cu^{II}$ centers are in a similar orientation to that in the aqua complex, that is, along the magic angles, while the formation of a hydroxo bridge leads to a reorientation of the $Cu^{II}$ centers and the macrocyclic backbone, such that a typical dipole−dipole coupled EPR spectrum emerges.

$$H = \beta_e \mathbf{B}\cdot\mathbf{g}\cdot\mathbf{S} + \mathbf{S}\cdot\mathbf{A}(^{63,65}Cu)\cdot\mathbf{I}(^{63,65}Cu) - \mathbf{g}_n\beta_n\mathbf{B}\cdot\mathbf{I} + \sum_{j=1}^{3}(\mathbf{S}_j\cdot\mathbf{A}_j(^{14,15}N)\cdot\mathbf{I}_j(^{14,15}N) - \mathbf{g}_n\beta_n\mathbf{B}_j\cdot\mathbf{I}_j(^{14,15}N)) \quad (1)$$

$$H = \sum_{i,j=1;1\neq j}^{2} H_i + J_{iso,ij}\mathbf{S}_i\cdot\mathbf{S}_j + \mathbf{S}_i\cdot J_{ij}\cdot\mathbf{S}_j \quad (2)$$

This interpretation was validated with the simulation of the EPR spectra. In general, the spectra are consistent with a square-pyramidal coordination environment of the $Cu^{II}$ centers in the mono- and dinuclear complexes ($d_{x^2-y^2}$ ground state, see also DFT section). The formally forbidden $\Delta m_S = \pm 2$ transitions at half field, as expected, could not be resolved from the spectra of the unbridged dinuclear complexes $[Cu^{II}_2(H_2pat^1)(H_2O)]^{2+}$ and $[Cu^{II}_2(H_2pat^1)(OH)]^{+}$ (note that the number of coordinated solvent molecules is uncertain): the already low transition probability is reduced by a further order of magnitude due to the orientation of the $Cu^{II}$ ions along the magic angles.[25] The experimental first derivative EPR spectra of these two species are shown in Figure 4a,c. After differentiation and Fourier and Savitzky−Golay filtering, second derivative spectra with resolved superhyperfine coupling $\mathbf{A}(^{14,15}N)$ due to the coordinated $N_{het}$ and $N_{amide}$ nitrogen atoms were obtained (Figure 4b,e).


dx.doi.org/10.1021/ic2004694 |Inorg. Chem. 2011, 50, 5165–5174

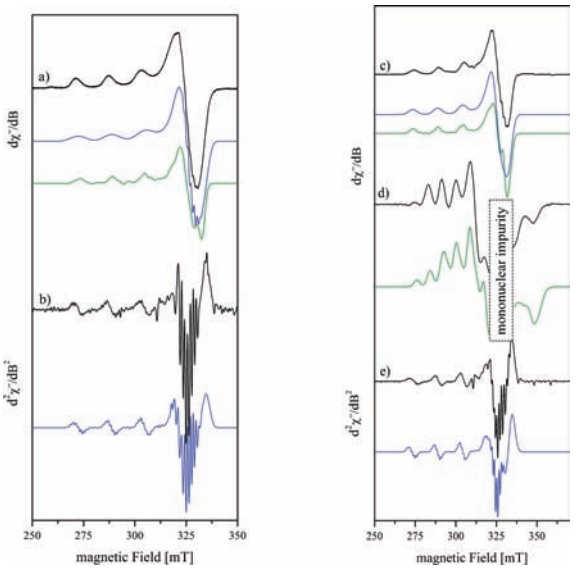


**Figure 4.** Experimental (black) and simulated (XSophe, blue; Molecular Sophe, green) X-band EPR spectra (MeOH, $c(H_4pat^1) = 1.25$ mM): (a) first derivative spectrum of $[Cu^{II}_2(H_2pat^1)(OH_2)]^{2+}$, $H_4pat^1/Cu^{II}/MeO^-$ 1:2:2; $T = 4.5$ K, $\nu = 9.375067$ GHz; (b) second derivative of spectrum a; (c) first derivative spectrum of $[Cu^{II}_2(H_2pat^1)(OH)]^{+}$, derived from spectral subtraction, $T = 50$ K, $\nu = 9.375402$ GHz; (d) $[Cu^{II}_2(H_2pat^1)(\mu\text{-}OH)(H_2O)_2]^{+}$, $T = 50$ K, $\nu = 9.375402$ GHz (see Supporting Information for simulation including the mononuclear impurity part); (e) second derivative spectrum of spectrum c.

The "apparent mononuclear spectra" were first simulated with the program package XSophe-Sophe-XeprView,[43] based on the spin Hamilton of eq 1. A mononuclear species was assumed in order to correctly determine the **g**, **A**($^{63}$Cu), and **A**($^{14}$N) hyperfine matrices. For the accurate simulation of the observed hyperfine resonances, two magnetically equivalent heterocyclic nitrogen nuclei and one amide nitrogen nucleus had to be included in the simulation (Table 1). The parameters were fitted with the quadratic variation of the Hooke and Jeeves method to the experimental spectrum and show excellent agreement with the experimental spectra with a mean least-squares error of 0.04. These spin Hamiltonian parameters were then used in a subsequent refinement with the program Molecular Sophe,[44] based on the coupled spin Hamiltonian (eq 2), which includes the individual spin Hamiltonians (eq 1) for each $Cu^{II}$ ion and the isotropic and anisotropic exchange terms. With Molecular Sophe, the anisotropic exchange splitting, the dipole−dipole coupling, and the relative orientation of the $Cu^{II}$ centers was obtained. The $g_{\|}$ and $A_{\|}$ values of $Cu^{II}$ complexes depend on the charge of the complex and on the number and nature of the coordinating atoms.[45] Therefore, the $g_{\|}$ and $A_{\|}$ values of the hydroxo $[Cu^{II}_2(H_2pat^1)(OH)]^{+}$ and aqua complex $[Cu^{II}_2(H_2pat^1)(OH_2)]^{2+}$ are slightly different. From the "apparent mononuclear EPR spectrum", we know that the two $Cu^{II}$ centers are oriented along the magic angles and that there is no significant structural rearrangement.

The simulation of the two "apparent mononuclear spectra" confirms the nearly identical geometries of these complexes (see Table 1). Both terminal aqua and hydroxo dinuclear complexes have a small anisotropic exchange splitting (0.0935 and 0.0938 $cm^{-1}$, respectively) and a close to zero ($4 \times 10^{-5}$ $cm^{-1}$) dipole−dipole coupling. The contribution of the anisotropic exchange coupling is small and the **g** and **A** matrices therefore must have similar orientations. The bridged hydroxo complex on the other hand has a large anisotropic exchange coupling ($(E/D)_{exc} = 0.20$ $cm^{-1}$) confirming a substantially different coordination geometry, where the $Cu^{II}$ centers are reoriented and the **g** and **A** matrices of both centers have significantly different orientations. Suitable crystals for X-ray analysis were obtained from the hydroxo-bridged complex, where a strong twist of the $Cu^{II}$ planes is visible (see below).

The unusual EPR features of the terminal aqua and hydroxo complexes of $H_4pat^1$ are reminiscent of those of the unbridged dinuclear $Cu^{II}$ complex of $H_4$patD, $[Cu^{II}_2(H_2patD)]^{2+}$.[25] This complex also has an "apparent mononuclear EPR spectrum", while the chloro-, hydroxo-, and carbonato-bridged dinuclear $Cu^{II}$ complexes of $H_4$patD are dipole−dipole coupled.[18] The simulated **g** and **A** values of the "apparent mononuclear complex" of $H_4$patD are very similar to those of the terminal complexes of $H_4pat^1$, emphasizing the suitability of $H_4pat^1$ as a model for patellamides (Table 1). The derived $Cu^{II}\cdots Cu^{II}$ distance in $[Cu^{II}_2(H_2patD)]^{2+}$ is considerably larger than that of the terminal aqua and hydroxo complexes of $H_4pat^1$ (6.8 vs. 4.0 Å); this probably is an artifact, caused by the neglect of the anisotropic exchange interaction in the simulation of the "apparent mononuclear spectrum" of $[Cu^{II}_2(H_2patD)]^{2+}$.[47]

*2.2.4. Structural Investigations of the Metal-Free Macrocycle and Its $Cu^{II}$ Complexes.* Single crystals of $H_4pat^1$ and its dinuclear copper(II) complex $[Cu^{II}_2(H_2pat^1)(\mu\text{-}OH)(H_2O)_2]ClO_4$ were obtained and analyzed by X-ray diffraction. In order to rationalize these structures and the solution properties, the structural data is compared with those of $H_4$patD, $H_4$asc, and the dinuclear $Cu^{II}$ complex of $H_4$asc $[Cu^{II}_2(H_2asc)(\mu\text{-}CO_3)]$.

In the solid-state $H_4$asc adopts a $C_2$-symmetric conformation, and a high degree of symmetry ($S_4$) is also present in $H_4pat^1$. As expected for symmetrical patellamide derivatives, $H_4pat^1$ adopts a square conformation, where the nitrogen atoms occupy the corners of a rectangle (Figures 1 and 5).

Differences in the macrocycle conformation arise from the variation of the heterocycles. The dimethyl-imidazole rings of $H_4pat^1$ are less flexible than the oxazoline rings of $H_4$asc and enforce a less folded conformation of the macrocycle (Figure 5). The differences in the folding may be quantified by the size of the macrocycle's cavity (distances between the nitrogen donors) and by the dihedral angle $\chi(N_{amide}-C_\alpha-C_{azole}-N_{het})$, see Table 2: the *trans*-disposed $N_{amide}$ nitrogen atoms of $H_4$asc are 7.13 Å (D-valine) and 5.28 Å (L-leucine) apart, while those of $H_4pat^1$ are equidistant (7.19 Å, X-ray; 6.59 Å, DFT-optimized structure, see Supporting Information). Interestingly, the $Cu^{II}$ coordination chemistry of the cyclic pseudo-octapeptides is not much affected by these structural differences, that is, the solution equilibria are very similar. The smaller distance of the *trans*-disposed $N_{amide}$ nitrogens in $H_4$asc and $H_4$patD must be the result of the more flexible oxazoline rings. $H_4pat^1$ and $H_4$asc both have two binding sites, where $Cu^{II}$ can either coordinate to an $N_{het}-N_{R\text{-}amide}-N_{het}$ or an $N_{het}-N_{S\text{-}amide}-N_{het}$ binding motif. The resulting mono- and dinuclear $Cu^{II}$ complexes of $H_4pat^1$ are enantiomers, while those of $H_4$asc are diastereomeric.

Single crystals of the racemic complex $[Cu^{II}_2(H_2pat^1)(\mu\text{-}OH)(H_2O)_2]ClO^-_4$ suitable for an X-ray structure analysis were isolated. In the crystal, both $Cu^{II}$ centers of each enantiomer have a square pyramidal coordination geometry, as predicted by the analysis of the EPR data. Two heterocyclic nitrogen atoms, a deprotonated amide nitrogen atom, and the oxygen atom of the bridging hydroxide form the equatorial planes, while the apical


dx.doi.org/10.1021/ic2004694 |*Inorg. Chem.* 2011, 50, 5165–5174

**Table 2. Selected Angles and Distances of the Metal Free Macrocycles and the Dinuclear $Cu^{II}$ Complexes of $H_4pat^1$, $H_4patD$, and $H_4asc$[25,26]**

| | $H_4pat^1$ | $H_4patD$ | $H_4asc$ | $[Cu^{II}_2(H_2pat^1)(\mu\text{-}OH)(H_2O)_2]^+$ | $[Cu^{II}_2(H_2asc)(\mu\text{-}CO_3)]$[26] |
|---|---|---|---|---|---|
| *trans*-disposed $N_{amide}$ [Å] | 7.19 | 7.80[a]/3.88 | 7.13[a]/5.27 | 6.735[c]/5.558 | 5.893[c]/6.294 |
| *trans*-disposed $N_{het}$ [Å] | 6.90 | 3.84[b]/7.48 | 6.41[b]/6.51 | 6.02/5.48 | 6.07/6.18[b] |
| consecutive $N_{amide}$ [Å] | 4.96 | 4.16/4.88/4.18/4.93 | 5.22/5.03 | 5.09/5.15 | 5.25/4.74/5.34/5.47 |
| $\chi[N_{amide}-C_\alpha-C_{azole}-X]$, deg | 133 | 168[b]/121 | 131[b]/155 | 128/169[c] | 117/153[c] |
| $\rho$ (angle between binding sites), deg | 78 | [d] | 34 | 77 | 49 |
| $Cu^{II}\cdots Cu^{II}$ [Å] | | | | 3.63 | 4.301 |

[a] *R** configuration at $C_\alpha$. [b] Thiazole $N_{het}$. [c] Coordinated. [d] Not in square conformation.

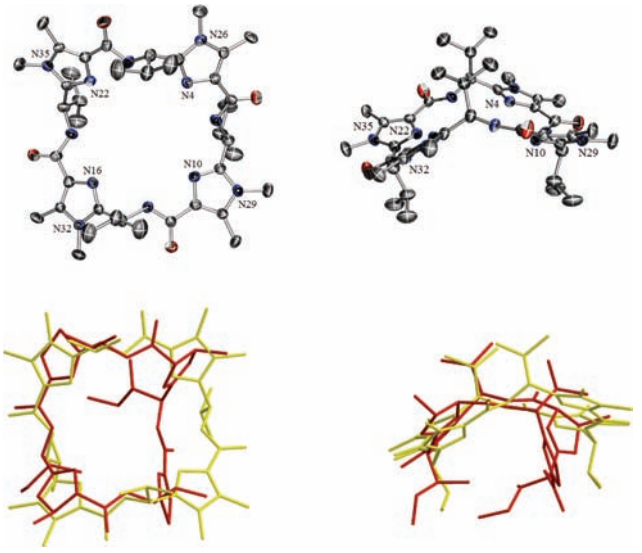


**Figure 5.** (top) ORTEP plot of the X-ray structure of $H_4pat^1$ from top (left) and side view (right). Ellipsoids are drawn at 50% probability (hydrogen atoms and solvent molecules are omitted for clarity, C = gray, N = blue, O = red. (bottom) Overlay plots of the X-ray structures of $H_4pat^1$ (yellow) and $H_4asc$ (red) from top (left) and side view (right).[48]

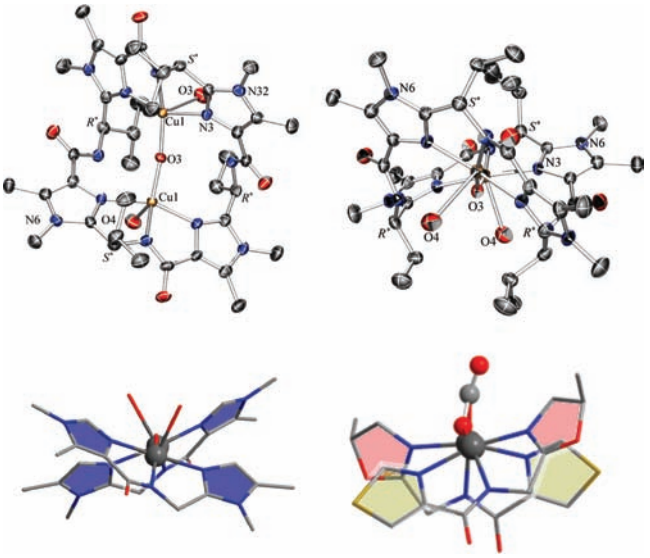


**Figure 6.** (top) ORTEP plot of the *S** enantiomer of the crystal structure of the hydroxo-bridged cation $[Cu^{II}_2(H_2pat^1)(\mu\text{-}OH)(H_2O)_2]^+$ from top (left) and side view (right). Ellipsoids are drawn at 50% probability; hydrogen atoms and solvent molecules are omitted for clarity; C = gray, N = blue, O = red, Cu = yellow; see Supporting Information for further crystallographic information. (bottom) Schematic representation of the twist of the binding sites in the hydroxo-bridged complex of $H_4pat^1$ (left) and the carbonato-bridged complex of $H_4asc$ (right); dimethyl-imidazole ring, blue; oxazoline ring, red; thiazole ring, ochre.

positions of both $Cu^{II}$ ions are occupied by water molecules at distances of 2.51 Å (Figure 6). The bridging hydroxide is equidistant (1.93 Å) from the $Cu^{II}$ centers. From the X-ray structure, a large twist of the $Cu^{II}$ planes of the bridged hydroxo complex emerges: the *z*-axes of the $Cu^{II}$ centers are rotated, and the *xy* planes of the $Cu^{II}$ centers are twisted. This is visualized in Figure 6: the *z*-axes coincide with the coordinated water molecules, and the *xy* plane of Cu1 is twisted with respect to that of Cu2 in a counterclockwise orientation. The Cu−O−Cu angle of 140.13° enforces a twist between the two $CuN_3$ planes (rotation around the $Cu\cdots Cu$ axis of around 38° in addition to the Cu−O−Cu angle of 140°), and this results, as expected, in a small isotropic exchange coupling (Table 1).[49]

In addition to the analysis of the X-ray data, the structures of the mono- and dinuclear $Cu^{II}$ complexes of $H_4pat^1$ were geometry-optimized using DFT (density functional theory, in the gas phase and in MeOH); the conformational space of the metal-free macrocycle $H_4pat^1$ was also analyzed by force field methods (molecular mechanics and molecular dynamics calculations). In general, the $Cu^{II}$ coordination sphere of the mononuclear $Cu^{II}$ complexes was completed by two water molecules.

The conformational analysis of the metal-free macrocycle revealed that it is not possible for $H_4pat^1$ to adopt a similar structure to those of $H_4asc$ or $H_4patD$, because the incorporated dimethyl-imidazole rings introduce severe steric constraints. However, although $H_4pat^1$ is less flexible than the natural macrocycles, the solution studies described above indicate that the $Cu^{II}$ coordination chemistry is only slightly affected.

Consistent with the simulated EPR spectra, the mono- and dinuclear $Cu^{II}$ complexes were found to have a distorted square-pyramidal coordination sphere, where the equatorial ligating atoms involve two imidazole nitrogens ($N_{het}$), one amide nitrogen ($N_{amide}$), and one oxygen of a coordinated water molecule. The water molecule at the apical position has a longer Cu1−O2 distance (2.29 Å) than the water coordinated in the equatorial plane (Cu1−O1 = 2.04 Å). The DFT analysis of the corresponding ligand conformations suggests that the ligand conformation of the hydroxo-bridged complex is


dx.doi.org/10.1021/ic2004694 |*Inorg. Chem.* 2011, 50, 5165–5174

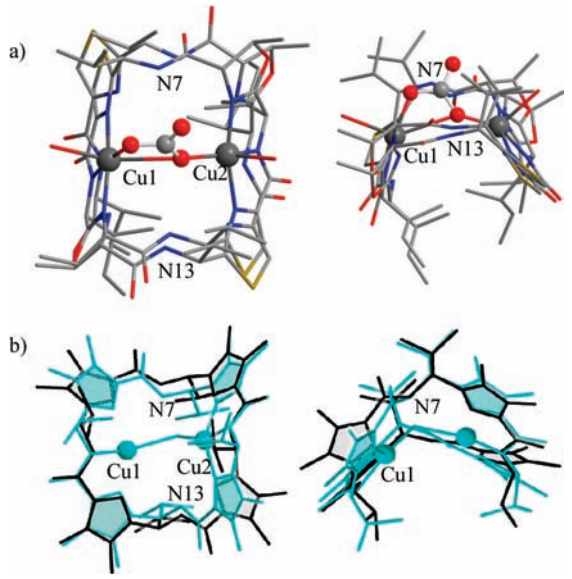


**Figure 7.** Top (left) and side views (right) of the following overlay plots: (a) $H_4$asc and $[Cu^{II}_2(H_2asc)(\mu\text{-}CO_3)]$ (X-ray structures); (b) X-ray structure of $H_4pat^1$ (black) with its computed (G09, B3LYP/6-31g*/TZVP, turquoise) dinuclear $Cu^{II}$ complex $[Cu^{II}_2(H_2pat^1)(\mu\text{-}OH)(H_2O)_2]^+$.

25 kJ/mol more stable than that of the mononuclear complex, explaining the preferred formation of dinuclear complexes (see Supporting Information for computational details and energies). A comparison of the X-ray structures of $H_4$asc and its dinuclear carbonato-bridged complex with the DFT-optimized and X-ray structures of $H_4pat^1$ reveals similarities and important differences between the systems. Both macrocycles have a high degree of preorganization for the formation of dinuclear complexes; this can be seen when the structures of the metal-free macrocycles are overlaid with those of their mono- and dinuclear $Cu^{II}$ complexes (see Figure 7; further overlay plots are given in the Supporting Information). However, there are significant differences between the structures of $H_4$asc and $H_4pat^1$, as well as between those of their dinuclear complexes. These are visualized in Figures 5, 6, and 7 and are primarily related to the tighter folding of the natural metal-free macrocycle, compared with the imidazole-derived synthetic ligand, and the resulting differences in the relative orientation of the two $Cu^{II}$ sites (distance and twist of the planes). From the experimental and computed structures, it also emerges that both ligands are highly preorganized, that binding of a first $Cu^{II}$ ion increases the preorganization for the second, and that the resulting structure of the ligand backbone and the two $Cu^{II}$ sites in the case of $H_4$asc is well suited for a bridging carbonate (three-atom bridge, Cu···Cu = 4.3 Å), while with $H_4pat^1$, the dinuclear complex is preorganized for the much smaller hydroxo bridge (one-atom bridge, Cu···Cu = 3.6 Å). Formation of carbonato-bridged complexes with $H_4pat^1$ could not be observed.

## 3. CONCLUSION

The substitution of the oxazoline and thiazole heterocycles of patellamides by dimethyl-imidazoles leads to rigidified macrocycles that retain most characteristics of the natural systems. In the solid state and in solution, the macrocycle $H_4pat^1$ adopts a conformation very similar to that of symmetrical patellamides such as $H_4$asc. Analysis of the X-ray structures in combination with DFT calculations and spectroscopic investigations showed that the lower flexibility does not strongly influence the preorganization of the macrocycle for the formation of dinuclear $Cu^{II}$ complexes, suggesting that this is a general feature of cyclic pseudo-octapeptides and that dinuclear $Cu^{II}$ complexes are related to the metabolic role of patellamides. Further suggestions related to the biological role of these complexes (e.g., carbonate fixation or oxygen activation) are purely speculative at this stage.

$H_4pat^1$ is able to model the unusual EPR features of the dinuclear $Cu^{II}$ complex of $H_4$patD. The orientation of the $Cu^{II}$ centers along the magic angles in combination with a small zero field splitting and a small anisotropic exchange coupling leads to "apparent mononuclear" EPR spectra as a result of the negligible dipole−dipole coupling in the unbridged dinuclear $Cu^{II}$ complexes.

Differences between the dimethyl-imidazole analogue $H_4pat^1$ and the natural systems were observed for the conformation of the macrocycle in the dinuclear complexes, that is, the orientation of the $Cu^{II}$ planes with respect to each other, and in the nature of the bridging anion. $H_4$asc and $H_4$patD form dinuclear carbonato-bridged complexes, while no carbonato complex could be observed for $H_4pat^1$. Instead $H_4pat^1$ forms a hydroxo-bridged complex. It is likely that the bridging anion depends on the incorporated heterocycles and that $H_4pat^1$ is too rigid to be bridged by a larger anion than hydroxide. The flexibility of thiazole and oxazoline heterocyclic rings in comparison to the dimethyl-imidazole rings may explain why Nature has chosen the thiazole−oxazoline combination for the patellamides and ascidiacyclamide.

## 4. EXPERIMENTAL SECTION

**4.1. Materials.** All solvents (absolute) and reagents (purum grade) were obtained commercially (Aldrich, Fluka) and were used without further purification. Analytical data of the intermediate compounds are given as Supporting Information.

**4.2. Synthesis of Methyl 2-((*R*)-2-(*tert*-Butoxycarbonylamino)-3-methylbutanamido)-3-oxobutanoate (2).** (*R*)-Boc-Val-OH (3.5 g, 15.6 mmol, 1 equiv) was dissolved in 100 mL of THF, NMM (*N*-methylmorpholine, 1.7 g, 16.65 mmol, 1 equiv) was added, and the solution was cooled to −25 °C. Subsequently isobutyl chloroformate (2.13 g, 15.6 mmol, 1 equiv) was added, during which the reaction mixture was maintained at −25 °C. After 35 min, the ammonium chloride salt **1**[50] (2.6 g, 15.6 mmol, 1 equiv), followed by a second equivalent of NMM (1.7 g, 47.8 mmol, 1 equiv) were added at −25 °C and stirring was continued for 20 h as the mixture was allowed to warm to room temperature. The solvent was evaporated, and the residue was dissolved in ethyl acetate and then washed with water and brine. The combined organic layers were dried over $MgSO_4$ and concentrated in vacuo. After recrystallization from ethyl acetate, 4.5 g of **2** were obtained as colorless crystals (87%). $C_{15}H_{26}N_2O_6$: calcd (%) C 54.53, H 7.93, N 8.48; found (%) C 54.66, H 7.94, N 8.62. $^1$H NMR (200 MHz, $CDCl_3$): $\delta$ = 0.87 (d, $^3J_{H,H}$ = 6.9 Hz, 3H, $CHCH_3$), 0.88 (d, $^3J_{H,H}$ = 6.9 Hz, 3H, $CHCH_3$), 0.93 (d, $^3J_{H,H}$ = 6.8 Hz, 6H, $CHCH_3$), 1.39(s, 9H, $C(CH_3)_3$), 1.40 (s, 9H, $C(CH_3)_3$), 2.10−2.26 (m, 2H, $CH(CH_3)_2$), 2.33 (s, 6H, $COCH_3$), 3.76 (s, 6H, $CO_2CH_3$), 4.0−4.08 (m, 2H, CHCONH), 5.07 (d, $^3J_{H,H}$ = 8.1 Hz, 1H, $NHCO_2$), 5.09 (d, $^3J_{H,H}$ = 8.6 Hz, 1H, $NHCO_2$), 5.21 (d, $^3J_{H,H}$ = 6.3 Hz, 2H, $CHCO_2$), 7.13 (d, $^3J_{H,H}$ = 6.3 Hz, 1H, NH), 7.18 (d, $^3J_{H,H}$ = 6.5 Hz, 1H, NH) ppm. $^{13}$C NMR (50 MHz, $CDCl_3$): $\delta$ = 17.3, 17.5 ($CH(CH_3)_2$), 19.1, 19.2 ($CH(CH_3)_2$), 27.9, 28.0 ($COCH_3$), 28.2 ($C(CH_3)_3$), 30.7, 30.9 ($CH(CH_3)_2$), 53.2, 53.3


dx.doi.org/10.1021/ic2004694 |*Inorg. Chem.* 2011, 50, 5165–5174

($CO_2CH_3$), 59.4, 59.5 (NHCHCO), 62.8, 62.9 ($NHCHCO_2$), 80.1 ($C(CH_3)_3$), 155.7 ($NHCOC(CH_3)_3$), 166.3, 166.4 ($CO_2CH_3$), 171.6 (NHCO), 198.0, 198.1 ($COCH_3$) ppm. FAB-HR MS: $m/z$ calcd for $C_{15}H_{27}N_2O_6^+$ 331.1866, found 331.1853. Mp: 106 °C.

**4.3. Synthesis of (*R*)-Methyl 2-(1-(*tert*-Butoxycarbonylamino)-2-methylpropyl)-1,5-dimethyl-imidazole-4-carboxylate (3).** Both glacial acetic acid (7.9 mL, 33.5 mmol, 1 equiv) and $NH_2Me$ in MeOH (8 M, 6.45 mL, 62.96 mmol, 4 equiv) were added to a solution of **2** (5.2 g, 15.7 mmol, 1 equiv) in 200 mL of xylene at room temperature. The solution was stirred at 155 °C with azeotropic removal of water for 8 h and then cooled to room temperature. The solvent was concentrated, and the residue was dissolved in AcOEt, and then washed with saturated $NaHCO_3$ solution and brine. The organic layer was dried over $Na_2SO_4$ and concentrated in vacuo. Purification was achieved by performing chromatography with silica gel (petroleum ether/ethyl acetate 1:3) to provide 3.6 g of **3** (72%) as a white solid. $C_{16}H_{27}N_3O_4$ (325.40): calcd (%) C 59.06, H 8.36, N 12.91; found (%) C 58.82, H 8.36, N 12.86. $^1$H NMR (200 MHz, $CDCl_3$): $\delta$ = 0.74 (d, $^3J_{H,H}$ = 6.7 Hz, 3H, $CHCH_3$), 0.93 (d, $^3J$ = 6.7 Hz, 3H, $CHCH_3$), 1.31 (s, 9H, $C(CH_3)_3$), 2.02−2.30 (m, 1H, $CH(CH_3)_2$), 2.44 (s, 3H, $C_{het}CH_3$), 3.48 (s, 1H, $NCH_3$), 3.79 (s, 1H, $CO_2CH_3$), 4.45 (dd, $^3J_{H,H}$ = 9.18 Hz, 1H, $C_\alpha H$), 5.26 (d, $J_{H,H}$ = 9.58 Hz, 1H, NH) ppm. $^{13}$C NMR (50 MHz, $CDCl_3$): $\delta$ = 10.2 ($C_{het}CH_3$), 18.5, 19.6 ($CH(CH_3)_2$), 28.3 ($C(CH_3)_3$), 30.3 ($NCH_3$), 33.2 ($CH(CH_3)_2$), 51.4 ($CO_2CH_3$), 52.1 ($C_\alpha$), 79.4 ($C(CH_3)_3$), 127.5 ($C_{het}CO_2$), 135.9 ($C_{het}CH_3$), 148.4 ($C_{het}N$), 155.6 (NHCO), 164.2 ($CO_2CH_3$) ppm. ESI-HR MS: $m/z$ calcd for $C_{16}H_{28}N_3O_4^+$ 326.2074, found 326.2075. Mp: 106 °C.

**4.4. Synthesis of (*R*)-2-(1-(*tert*-Butoxycarbonylamino)-2-methylpropyl)-1,5-dimethyl-imidazole-4-carboxylic acid (4).** Compound **3** (1.9 g, 5.8 mmol) was converted into **4**, using 29 mL of NaOH, 0.1 M, in 73 mL of a dioxane/methanol mixture. $C_{15}H_{25}N_3O_4$ (311.38): calcd (%) C 59.06, H 8.36, N 12.91; found (%) C 58.82, H 8.36, N 12.86. $^1$H NMR (200 MHz, $CDCl_3$): $\delta$ = 0.74 (d, $^3J_{H,H}$ = 6.7 Hz, 3H, $CHCH_3$), 1.11 (d, $^3J_{H,H}$ = 6.6 Hz, 3H, $CHCH_3$), 1.35 (s, 9H, $C(CH_3)_3$), 2.48−2.62 (m, 1H, $CH(CH_3)_2$), 2.58 (s, 3H, $C_{het}CH_3$), 3.67 (s, 3H, $NCH_3$), 4.55 (dd, $^3J_{H,H}$ = 9.33 Hz 1H, $C_\alpha H$), 7.40 (s, 1H, $NHCO_2$), 10.67 (s, 1H, $CO_2H$) ppm. $^{13}$C NMR (50 MHz, $CDCl_3$): $\delta$ = 9.7 ($C_{het}CH_3$), 19.4, 19.6 ($CH(CH_3)_2$), 28.2 ($C(CH_3)_3$), 31.8 ($CH(CH_3)_2$), 32.3 ($NCH_3$), 52.6 ($C_\alpha$), 79.9 ($C(CH_3)_3$), 123.4 ($C_{het}CO_2$), 135.1 ($C_{het}NCH_3$), 149.0 ($C_{azole}$), 156.2 ($CO_2NH$), 161.3 ($CO_2H$) ppm. FAB-HR MS: $m/z$ calcd for $C_{15}H_{26}N_3O_4^+$ 312.2074, found 312.2088. Mp: 104 °C.

**4.5. Synthesis of Methyl 2-((*S*)-1-(2-((*R*)-1-(*tert*-Butoxycarbonylamino)-2-methylpropyl)-1,5-dimethyl-imidazole-4-carboxamido)-2-methylpropyl)-1,5-dimethyl-imidazole-4-carboxylate (5).** FDPP (pentafluorophenyl diphenylphosphinate, 3.50 g, 9.12 mmol) and EDIPA (ethyldiisopropylamine, 5.7 mL, 31.2 mmol) were added at room temperature to a solution of **4** (1.50 g, 4.80 mmol) and (*S*)-TFA-Val-imidazole-methoxide (2.40 g, 7.20 mmol) in 150 mL of acetonitrile, and the mixture was stirred at room temperature for 4 days. The solvent was then evaporated, and the residue was dissolved in ethyl acetate. The organic layers were washed with water and brine, dried with $MgSO_4$, and concentrated in vacuo. Flash chromatography on silica gel (petrol ether:ethyl acetate 1:2) gave **5** (1.7 g, 68%) as a white solid. $C_{26}H_{42}N_6O_5 \cdot H_2O$: calcd (%) C 58.19, H 8.26, N 15.66; found (%) C 58.53, H 8.08, N 14.70. $^1$H NMR (400 MHz, $CDCl_3$): $\delta$ = 0.82 (d, $^3J_{H,H}$ = 6.9 Hz, 3H, $CHCH_3$), 0.84 (d, $^3J_{H-H}$ = 6.7 Hz, 3H, $CHCH_3$), 0.94 (d, $^3J_{H,H}$ = 6.7 Hz, 3H, $CHCH_3$), 1.06 (d, $^3J_{H,H}$ = 6.55 Hz, 3H, $CHCH_3$), 1.44 (s, 9H, $C(CH_3)_3$), 1.99−2.13 (m, 1H, $CHCH_3$), 2.51 (s, 6H, $C_{het}CH_3$), 2.52−2.62 (m, 1H, $CHCH_3$), 3.47 (s, 3H, $NCH_3$), 3.64 (s, 3H, $NCH_3$), 3.85 (s, 3H, $CO_2CH_3$), 4.51 (dd, $^3J_{H,H}$ = 8.57 Hz, 1H, $C_\alpha H$), 4.96 (dd, $^3J_{H,H}$ = 9.85 Hz, 1H, $C_\alpha H$), 5.36−5.22 (m, 1H, NH), 7.68 (m, 1H, NH) ppm. $^{13}$C NMR (100 MHz, $CDCl_3$): $\delta$ = 9.7, 10.2 ($C_{het}CH_3$), 18.1, 19.2, 19.6, 20.0 ($CHCH_3$), 28.3 ($CCH_3$), 30.0, 30.4 ($CH(CH_3)_2$), 32.3, 32.9 ($NCH_3$), 52.1 ($CO_2CH_3$), 79.5 ($C(CH_3)_3$), 135.9, 146.9, 148.3 ($C_{het}$), 155.7, 163.5, 163.7 (CO) ppm. FAB-HR MS: $m/z$ calcd for $C_{26}H_{43}N_6O_5^+$ 519.32894; found 519.3318. Mp: 179 °C.

**4.6. Synthesis of $H_4$pat$^1$.** Compound **5** (1.7 g, 3.26 mmol) was converted into the free acid, using 33 mL of NaOH in 40 mL of a dioxane/methanol mixture. The solution was stirred until TLC showed complete conversion, and then brine, 1 M HCl solution, and DCM were added. The aqueous phase was repeatedly extracted with DCM, and the organic layers were combined, dried with $MgSO_4$, and concentrated in vacuo. The free acid was used in the following step without further purification. The Boc group was removed using 8.7 mL of TFA in 58 mL of DCM. The solution was kept at 0 °C upon addition of TFA. Stirring was continued for 3 h. The mixture was concentrated in vacuo to provide a quantitative yield of the trifluoroacid salt. Remaining solvent and TFA were removed through repetitive stripping with EtOAc. The resulting salt was then washed with ice cold DCM. The TFA−diimidazoleacid (1.5 g, 2.11 mmol) was then cyclodimerized using EDIPA (1.87 g, 14.77 mmol) and FDPP (2.23 g, 5.8 mmol) in an acetonitrile suspension. The mixture was stirred at room temperature for 2 days. The solvent was evaporated, and the residue was dissolved in EtOAc, then extracted with water and brine, dried with $MgSO_4$, and concentrated in vacuo. Flash chromatography on silica gel (DCM:EtOAc:MeOH 70:30:4) gave $H_4$pat$^1$ in 51% yield (302 mg, 0.95 mmol). Slow evaporation of a methanolic $H_4$pat$^1$ solution provided colorless crystals suitable for X-ray diffraction. $C_{40}H_{60}N_{12}O_4 \cdot H_2O \cdot 1/2$ EtOAc: calcd (%) C 60.45, H 7.91, N 20.14; found (%) C 60.64, H 8.00, N 20.47 (28059). $^1$H NMR (750 MHz, $CDCl_3$): $\delta$ = 0.87 (d, $^3J_{H,H}$ = 6.75 Hz, 3H, $CH(CH_3)_2$), 0.92 (d, $^3J_{H,H}$ = 6.76 Hz, 3H, $CH(CH_3)_2$), 2.19−2.29 (m, 1H, $CHCH_3$), 2.55 (s, 3H, $C_{het}CH_3$), 3.64 (s, 3H, $NCH_3$), 5.11−5.14 (m, 1H, $C_\alpha H$), 8.60 (d, $^3J$ = 9.04 Hz, 1H, NH) ppm. $^{13}$C NMR (175 MHz, $CDCl_3$): $\delta$ = 9.8 ($C_{het}CH_3$), 18.7, 19.6 ($CH(CH_3)_2$), 30.7 ($CH(CH_3)_2$), 35.6 ($NCH_3$), 51.0 (NHCH), 130.1 ($C_{het}CO$), 134.5 ($C_{het}NCH_3$), 148.2 ($C_{azole}$), 165.4 (NHCO) ppm. FAB-HR MS: $m/z$ calcd for $C_{40}H_{61}N_{12}O_4^+$ 773.4939;, found 773.4944. Mp: >250 °C.

**4.7. Synthesis of $[Cu^{II}_2(H_2pat^1)(\mu\text{-}OH)(H_2O)]^+[ClO^-_4]$.** $H_4$pat$^1$ was dissolved in MeOH (10 mL), 4 equiv of ($n$-$Bu_4N$)(OMe) and 2 equiv of $Cu(Otf)_2$ were added, and the solution was stirred for 30 min. Water (5 mL) and small amounts of sodium perchlorate were added, and the solution was slowly evaporated to yield turquoise crystals, suitable for X-ray diffraction. The yield of crystals was too small for elemental analysis.

**4.8. Methods.** $^1$H and $^{13}$C NMR spectra were recorded with a Bruker 200 MHz DRX or a Bruker Avance 400 MHz. All chemical shifts ($\delta$) are given in ppm relative to TMS. The spectra were referenced to deuterated solvents, indicated in brackets in the analytical data.

Continuous-wave X-band (ca. 9 GHz) EPR spectra were recorded with a Bruker Biospin Elexsys E500 EPR spectrometer fitted with a super high Q cavity. The magnetic field and the microwave frequency were calibrated with a Bruker ER 034TM Teslameter and a Bruker microwave frequency counter, respectively. A flow-through cryostat in conjunction with a Eurotherm (B-VT-2000) variable-temperature controller provided temperatures of 127−133 K at the sample position in the cavity. For lower temperatures (4−52 K), an Oxford Instruments ESR 910 flow-through cryostat in conjunction with an ITC4 temperature controller was employed. Spectrometer tuning, signal averaging, and visualization were accomplished with Bruker's Xepr (version 2.503b.12) software. The EPR spectra of the mono- and dinuclear complexes were simulated with the XSophe-Sophe-XperView[43] (version 1.1.4) and Molecular Sophe[44] (version 2.0.91) computer simulation software suites on a personal computer, running with the Mandriva Linux v2007.0 operating system.

High-resolution electrospray ionization mass spectrometry (ESI-MS) was performed with a 9.4 T Bruker ApexQe Qh-ICR hybrid instrument with an Apollo II MTP ion source in the positive- and negative-ion electrospray ionization (ESI) mode. Sample solutions in methanol at

concentrations of $10^{-4}-10^{-5}$ M were admitted to the ESI interface by means of a syringe pump at 5 mL $min^{-1}$ and sprayed at 4.5 kV with a desolvation gas flow of 2.0 L $min^{-1}$ at 25 °C and a nebulizer gas flow of 1.0 L $min^{-1}$. The ions were accumulated in the storage hexapole for 0.1−1.0 s and then transferred into the ICR cell. Trapping was achieved at a sidekick potential of −4.0 V and trapping potentials of roughly 1 V. The mass spectra were acquired in the broadband mode with 1 M data points. Typically, 16 transients were accumulated for one magnitude spectrum. External mass calibration was performed on $[\text{arginine}_n + H]^+$ cluster ions prior to analysis. A mass accuracy of 1 ppm was achieved. The instrument was controlled by Bruker ApexControl 2.0.0.beta software, and data analysis was performed using Bruker Data Analysis 3.4 software.

Spectrophotometric titrations were performed in MeOH at 25.0 °C on 2 $cm^3$ samples at a $H_4pat^1$ concentration of 1.25 mM. Copper(II) triflate and base ($n$-$Bu_4N$)(OMe) were added stepwise in 0.1 (10 $\mu$L) or 0.2 (20 $\mu$L) equiv steps. The recorded spectra were corrected for the dilution factor.

UV−vis/NIR spectra were recorded with a JASCO V-570 spectrophotometer.

**4.9. X-ray Crystallography.** Suitable crystals of $H_4pat^1$ and of $[Cu^{II}_2(H_2pat^1)(\mu\text{-}OH)(H_2O)_2]ClO_4$ were mounted with perfluorinated polyether oil on the tip of a glass fiber and cooled immediately on the goniometer head to 200 K. Data collections were performed using a STOE IPDS diffractometer with Mo Kα radiation ($\lambda$ = 0.71073 Å). The structure was refined using the Bruker AXS SHELXTL 5.1 program package.[51] Refinement was in full-matrix least-squares against $F^2$. All noncarbon hydrogen atoms were taken from a difference Fourier map and refined with free isotopic $U$ values; carbon−hydrogen atoms were included as riding models with fixed isotropic $U$ values in the final refinement.

**4.10. Modeling.** DFT calculations were performed with Gaussian 03[52] and Gaussian 09.[53] Geometry optimizations were performed using the B3LYP[54−56] hybrid functional in combination with the basis sets 6-31g*[56] (C, H, N, O, S) and TZVP[57] (Cu). A frequency calculation was performed subsequent to the geometry optimization to confirm the structures as a minimum on the potential surface. In one instance, the PCM[58] solvation model with methanol as solvent was applied.

Molecular mechanics simulations were performed with Macromodel,[59] using the Amber force field. A 1000 step low-frequency-mode conformational search was performed to check for different conformations of $H_4pat^1$. After the conformational search, a multiple minimization was performed.

## ■ ASSOCIATED CONTENT

**Supporting Information.** Crystal structure data, computed structures, relevant experimental and simulated spectra not given in the paper, and analytical data of intermediates. This material is available free of charge via the Internet at http://pubs.acs.org.

## ■ AUTHOR INFORMATION

### Corresponding Author

*E-mail: peter.comba@aci.uni-heidelberg.de. Fax: +49-6226-546617.

## ■ ACKNOWLEDGMENT

Generous financial support by the University of Heidelberg and the German Science Foundation (DFG) are gratefully acknowledged. We thank Prof. Haberhauer (University of Duisburg-Essen), Prof. Gahan, and Dr. Noble (University of Queensland) for fruitful discussions and Thomas Zessin for support with the X-ray structure analyses.

## ■ REFERENCES

(1) Wipf, P.; M., C. P. *J. Am. Chem. Soc.* **1992**, *114*, 10975.
(2) van den Brenk, A. L.; Fairlie, D. P.; Hanson, G. R.; Gahan, L. R.; Hawkins, C. J.; Jones, A. *Inorg. Chem.* **1994**, *33*, 2280.
(3) Morris, L. A.; Jaspars, M.; Bosch, J. J. K.-v. d.; Versluis, K.; Heck, A. J. R.; Kelly, S. M.; Price, N. C. *Tetrahedron* **2001**, *57*, 3185.
(4) Milne, B. F.; Morris, L. A.; Jaspers, M.; Thompson, G. S. *J. Chem. Soc., Perkin Trans. 2* **2002**, 1076.
(5) Ikegami, F.; Murakoshi, I. *Phytochemistry* **1994**, *35*, 1089.
(6) Wang, M.; Gould, S. J. *J. Org. Chem.* **1993**, *58*, 5176.
(7) Ishida, T.; In, Y.; Shinozaki, F.; Doi, M.; Yamamoto, D.; Hamada, Y.; Shioiri, T.; Kamigauchi, M.; Sugiwra, M. *J. Org. Chem.* **1995**, *60*, 3944.
(8) McDonald, L. A.; Foster, M. P.; Phillips, D. R.; Ireland, C. M.; Lee, A. Y.; Clardy, J. *J. Org. Chem.* **1992**, *57*, 4616.
(9) Schmitz, F. J.; Ksebati, M. B.; Chang, J. S.; Wang, J. L.; Hossain, M. B.; van der Helm, D. *J. Org. Chem.* **1989**, *54*, 3463.
(10) Haberhauer, G.; Pinter, A.; Oeser, T.; Rominger, F. *Eur. J. Org. Chem.* **2007**, 1779.
(11) Haberhauer, G.; Rominger, F. *Tetrahedron Lett.* **2002**, *43*, 6335.
(12) Haberhauer, G.; Rominger, F. *Eur. J. Org. Chem.* **2003**, 3209.
(13) Schmidt, E. W.; Nelson, J. T.; Rasko, D. A.; Sudek, S.; Eisen, J. A.; Haygood, M. G.; Ravel, J. *Proc. Natl. Acad. Sci. U.S.A.* **2005**, *102*, 7315.
(14) Degnan, B. M.; Hawkins, C. J.; Lavin, M. F.; McCaffrey, E. J.; Parry, D. L.; Watters, D. J. *J. Med. Chem.* **1989**, *32*, 1354.
(15) Comba, P.; Cusack, R.; Fairlie, D. P.; Gahan, L. R.; Hanson, G. R.; Kazmaier, U.; Ramlow, A. *Inorg. Chem.* **1998**, *37*, 6721.
(16) Comba, P.; Gahan, L. R.; Haberhauer, G.; Hanson, G. A.; Noble, C. J.; Seibold, B.; van den Brenk, A. L. *Chem.—Eur. J.* **2008**, *14*, 4393.
(17) Bernhardt, P. V.; Comba, P.; Fairlie, D. P.; Gahan, L. R.; Hanson, G. R.; Lötzbeyer, L. *Chem.—Eur. J.* **2002**, *8*, 1527.
(18) van den Brenk, A. L.; Tyndall, J. D. A.; Cusack, R. M.; Jones, A.; Fairlie, D. P.; Gahan, L. R.; Hanson, G. R. *J. Inorg. Biochem.* **2004**, *98*, 1857.
(19) Grondahl, L.; Sokolenko, N.; Abberate, G.; Fairlie, D. P.; Hanson, G. R.; Gahan, L. R. *J. Chem. Soc., Dalton Trans.* **1999**, 1227.
(20) Wipf, P.; Wang, C. *Org. Lett.* **2006**, *8*, 2381.
(21) Wipf, P.; V., S.; Miller, C. P. *Angew. Chem.* **1994**, *106*, 1554.
(22) van den Brenk, A. L.; Byriel, K. A.; Fairlie, D. P.; Gahan, L. R.; Hanson, G. R.; Hawkins, C. J.; Jones, A.; Kennard, C. H. L.; Moubaraki, B.; Murray, K. S. *Inorg. Chem.* **1994**, *33*, 3549.
(23) Comba, P.; Gahan, L. R.; Haberhauer, G.; Hanson, G. R.; Noble, C. J.; Seibold, B.; van den Brenk, A. L. *Chem.—Eur. J.* **2008**, *14*, 4393.
(24) van den Brenk, A. L.; Hanson, G. R.; Hawkins, C. J. *J. Inorg. Biochem.* **1989**, *98*, 165.
(25) van den Brenk, A. L.; Fairlie, D. P.; Hanson, G. R.; Gahan, L. R.; Hawkins, C. J.; Jones, A. *Inorg. Chem.* **1994**, *33*, 2280.
(26) van den Brenk, A. L.; Byriel, K. A.; Fairlie, D. P.; Gahan, L. R.; Hanson, G. R.; Hawkins, C. J.; Jones, A.; Kennard, C. H. L.; Moubaraki, B.; Murray, K. S. *Inorg. Chem.* **1994**, *33*, 3549.
(27) Grondahl, L.; Sokolenko, N.; Abbenante, G.; Fairlie, D. P.; Hanson, G. R.; Gahan, L. R. *J. Chem. Soc., Dalton Trans.* **1999**, 1227.
(28) Cusack, R. M.; Grondahl, L.; Abbenante, G.; Fairlie, D. P.; Gahan, L. R.; Hanson, G. R.; Hambley, T. W. *J. Chem. Soc., Perkin Trans. 2* **2000**, 323.
(29) Wipf, P.; Miller, C. P. *J. Am. Chem. Soc.* **1992**, *114*, 10975.
(30) Haberhauer, G.; Pinter, A.; Oeser, T.; Rominger, F. *Eur. J. Org. Chem.* **2007**, 1779.
(31) Degnan, B. M.; Hawkins, C. J.; Lavin, M. F.; McCaffrey, E. J.; Parry, D. L.; van den Brenk, A. L.; Watters, D. J. *J. Med. Chem.* **1989**, *32*, 1349.

(32) Ishida, T.; In, Y.; Shinozaki, F.; Doi, M.; Yamamoto, D.; Hamada, Y.; Shioiri, T.; Kamigauchi, M.; Sugiura, M. *J. Org. Chem.* **1995**, *60*, 3944.
(33) Hamamoto, Y.; Endo, M.; Nakagawa, M.; Nakanishi, T.; Mizukawa, K. *J. Chem. Soc., Chem. Commun.* **1983**, 323.
(34) Hambley, T. W.; Hawkins, C. J.; Lavin, M. F.; van den Brenk, A.; Watters, D. J. *Tetrahedron* **1992**, *48*, 341.
(35) Morris, L. A.; Jaspars, M. *Spec. Publ.—R. Soc. Chem.* **2000**, *257*, 140.
(36) Ishida, T.; Tanaka, M.; Nabae, M.; Inoue, M.; Kato, S.; Hamada, Y.; Shioiri, T. *J. Org. Chem.* **1988**, *53*, 107.
(37) Schmitz, F. J.; Ksebati, M. B.; Chang, J. S.; Wang, J. L.; Hossain, M. B.; Van der Helm, D.; Engel, M. H.; Serban, A.; Silfer, J. A. *J. Org. Chem.* **1989**, *54*, 3463.
(38) Comba, P.; Dovalil, N.; Haberhauer, G.; Hanson, G. R.; Kato, Y.; Taura, T. *J. Biol. Inorg. Chem.* **2010**, *15*, 1129.
(39) Haberhauer, G. *Tetrahedron Lett.* **2008**, *49*, 2421.
(40) The coordinated water and hydroxide result from residual water in the solvent (methanol) and base.
(41) The intensities of the absorption bands at 685 and 550 nm show a plateau-like behavior (Figure 2d). One would expect an inflection point at the addition of 2 equiv of base; the plateau-like behavior is due to the overlap of the different species that contribute to the absorption bands and cover the inflection point.
(42) Note that the dinuclear spectrum contains small impurities of the apparent mononuclear complex, identifiable by the superhyperfine coupling present at ~320 mT. These could not be eliminated by spectra subtraction.
(43) Hanson, G. R.; Gates, K. E.; Noble, C. J.; Griffin, M.; Mitchell, A.; Benson, S. *J. Inorg. Biochem.* **2004**, *98*, 903.
(44) Hanson, G. R.; Noble, C. J.; Benson, S. *Biol. Magn. Res.* **2008**, *28*, 105.
(45) Blumberg, W. E.; Peisach, J. *Arch. Biochem. Biophys.* **1974**, *165*, 691.
(46) Poupko, R.; Luz, Z. *J. Chem. Phys.* **1972**, *57*, 3311.
(47) The simulated $Cu^{II}\cdots Cu^{II}$ distance in the chloro- and carbonato-bridged complexes of $H_4$patD are significantly smaller, and the macrocycle is unlikely to support such a large distance of the $Cu^{II}$ centers.
(48) Ishida, T.; In, Y.; Doi, M.; Inoue, M.; Hamada, Y.; Shioiri, T. *Biopolymers* **1992**, *32*, 131.
(49) Hodgson, D. J. *Prog. Inorg. Chem.* **1975**, *19*, 173.
(50) Singh, J.; Gordon, T. D.; Earley, W. G.; Morgan, B. A. *Tetrahedron Lett.* **1993**, *34*, 211.
(51) Sheldrick, G. M. SHELXTL 5.1, Bruker AXS, Inc. Madison, WI, 1994.
(52) Frisch, M. J.; Trucks, G. W.; Schlegel, H. B.; Scuseria, G. E.; Robb, M. A.; Cheeseman, J. R.; Montgomery, J. A., Jr.; Vreven, T.; Kudin, K. N.; Burant, J. C.; Millam, J. M.; Iyengar, S. S.; Tomasi, J.; Barone, V.; Mennucci, B.; Cossi, M.; Scalmani, G.; Rega, N.; Petersson, G. A.; Nakatsuji, H.; Hada, M.; Ehara, M.; Toyota, K.; Fukuda, R.; Hasegawa, J.; Ishida, M.; Nakajima, T.; Honda, Y.; Kitao, O.; Nakai, H.; Klene, M.; Li, X.; Knox, J. E.; Hratchian, H. P.; Cross, J. B.; Bakken, V.; Adamo, C.; Jaramillo, J.; Gomperts, R.; Stratmann, R. E.; Yazyev, O.; Austin, A. J.; Cammi, R.; Pomelli, C.; Ochterski, J. W.; Ayala, P. Y.; Morokuma, K.; Voth, G. A.; Salvador, P.; Dannenberg, J. J.; Zakrzewski, V. G.; Dapprich, S.; Daniels, A. D.; Strain, M. C.; Farkas, O.; Malick, D. K.; Rabuck, A. D.; Raghavachari, K.; Foresman, J. B.; Ortiz, J. V.; Cui, Q.; Baboul, A. G.; Clifford, S.; Cioslowski, J.; Stefanov, B. B.; Liu, G.; Liashenko, A.; Piskorz, P.; Komaromi, I.; Martin, R. L.; Fox, D. J.; Keith, T.; AlLaham, M. A.; Peng, C. Y.; Nanayakkara, A.; Challacombe, M.; Gill, P. M. W.; Johnson, B.; Chen, W.; Wong, M. W.; Gonzalez, C.; Pople, J. A. *Gaussian 03*, revision B.03; Gaussian, Inc.: Wallingford, CT, 2003.
(53) Frisch, M. J.; Trucks, G. W.; Schlegel, H. B.; Scuseria, G. E.; Robb, M. A.; Cheeseman, J. R.; Scalmani, G.; Barone, V.; Mennucci, B.; Petersson, G. A.; Nakatsuji, H.; Caricato, M.; Li, X.; Hratchian, H. P.; Izmaylov, A. F.; Bloino, J.; Zheng, G.; Sonnenberg, J. L.; Hada, M.; Ehara, M.; Toyota, K.; Fukuda, R.; Hasegawa, J.; Ishida, M.; Nakajima, T.; Honda, Y.; Kitao, O.; Nakai, H.; Vreven, T.; Montgomery, J. A., Jr.; Peralta, J. E.; Ogliaro, F.; Bearpark, M.; Heyd, J. J.; Brothers, E.; Kudin, K. N.; Staroverov, V. N.; Kobayashi, R.; Normand, J.; Raghavachari, K.; Rendell, A.; Burant, J. C.; Iyengar, S. S.; Tomasi, J.; Cossi, M.; Rega, N.; Millam, J. M.; Klene, M.; Knox, J. E.; Cross, J. B.; Bakken, V.; Adamo, C.; Jaramillo, J.; Gomperts, R.; Stratmann, R. E.; Yazyev, O.; Austin, A. J.; Cammi, R.; Pomelli, C.; Ochterski, J. W.; Martin, R. L.; Morokuma, K.; Zakrzewski, V. G.; Voth, G. A.; Salvador, P.; Dannenberg, J. J.; Dapprich, S.; Daniels, A. D.; Farkas, O.; Foresman, J. B.; Ortiz, J. V.; Cioslowski, J.; Fox, D. J. *Gaussian 09*, revision A.02; Gaussian, Inc.: Wallingford, CT, 2009.
(54) Becke, A. D. *Phys. Rev. A* **1988**, *38*, 3098.
(55) Lee, C. T.; Yang, W. T.; Parr, R. G. *Phys. Rev. B* **1988**, *37*, 785.
(56) Schafer, A.; Horn, H.; Ahlrichs, R. *J. Chem. Phys.* **1992**, *97*, 2571.
(57) Schafer, A.; Huber, C.; Ahlrichs, R. *J. Chem. Phys.* **1994**, *100*, 5829.
(58) *Modern Theoretical Chemistry*; Dunning, J. T. H., Hay, P. J., Eds.; Plenum: New York, 1976.
(59) Mohamadi, F.; Richards, N. G. J.; Guida, W. C.; Liskamp, R.; Lipton, M.; Caufield, C.; Chang, G.; Hendrickson, T.; Still, W. C. *J. Comput. Chem.* **1990**, *11*, 440.